Engineering Applications of Computational Fluid Mechanics, 2015
Vol. 9, No. 1, 419–431, http://dx.doi.org/10.1080/19942060.2015.1037993

Taylor & Francis
Taylor & Francis Group

RESEARCH ARTICLE

CFD study of capillary jets under superimposed destabilizing conditions for microdroplet formation

Cristina Rodriguez-Rivero[a,b], Eva M. Martin del Valle[a*] and Miguel A. Galán[a]

[a]*Department of Chemical Engineering, University of Salamanca, Spain;* [b]*Department of Engineering, University of Cambridge, UK*

(*Received 8 October 2014; final version received 2 April 2015*)

Initial numerical studies on the capillary laminar instability of continuous polymeric jets subjected to controlled destabilization and their comparison with experimental results obtained from a microparticle formation technique are addressed. Continuous jet instabilities and drop formation are challenging free-surface flow problems that require sophisticated interface tracking methods. The assessment of a Coupled Volume of Fluid and Level Set (CLSVOF) commercial code and its potential application to more complex systems are considered. The data obtained from the numerical simulations under different operating conditions showed good qualitative results, in agreement with the trends experimentally obtained. Nevertheless, the use of generalized Newtonian models instead of more complex constitutive equations accounting for the polymer viscoelasticity preclude the obtaining of better comparisons. However, it can be concluded that the use of CLSVOF under the described conditions deals reasonably well with the tracking of the interface, making its use adequate in capillary laminar instabilities.

Keywords: CFD; microdroplet; VOF; laminar instability; non-Newtonian; polymer

Introduction

The formation of microdroplets and microparticles with controlled features, mainly related to size and shape, is an important subject in the design of several processes such as inkjet printing (de Gans, Duineveld, & Schubert, 2004) microfluidic devices (Song, Chen, & Ismagilov, 2006; Srinivasan, Pamula, & Fair, 2004), cell encapsulation (Zimmermann et al., 2008), and powder and particulate systems for fine chemicals or pharmaceuticals (Alderliesten, 2004; Chan, Tan, & Heng, 2008).

Numerous methods for the generation of microparticles are available, in study or in development (Benita, 2006). This research group focuses on mechanical procedures that do not rely on sharp changes of temperature or toxic reagents, so that they are suitable for encapsulating biological ingredients, such as cells or proteins (Cerveró, Nogareda, Valle, & Galán, 2011; Rodriguez-Rivero, Del Valle, & Galán, 2011).

These processes are based on the breakup of capillary jets under different instabilization conditions. The different disintegration modes are usually classified following criteria derived from the values of Reynolds, Weber and Ohnesorge numbers (Pan & Suga, 2006; Reitz & Bracco, 1986). The cases of study covered in this work correspond to the laminar regime, given for low Reynolds numbers. Savart (1833) and Plateau (1873) studied this regime in cylindrical liquid jets and found that a surface-tension-driven instability at the interphase of the jet with the surrounding media was responsible for their axisymmetric breakup. Weber (1931) extended the study to consider viscous effects and after him other authors have studied more complex conditions (Bogy, 1979; Chigier & Reitz, 1996; Goedde & Yuen, 1970; Sterling & Sleicher, 1975). However, interfacial instabilities in jets are yet to be fully understood (Eggers, 2014; Eggers & Villermaux, 2008; Javadi, Eggers, Bonn, Habibi, & Ribe, 2013) and numerical studies have been conducted to help shed light on the phenomenon. In this sense, computational tools such as those embracing Computational Fluid Dynamics (CFD) are attracting increasing interest.

Continuous jet instabilities and drop formation are challenging free-surface flow problems that require sophisticated interface tracking methods. Several of these methods have been developed in the last decades. The Volume of Fluid (VOF) method was firstly implemented by Hirt and Nichols (1981) and is one of the most used methods for free-surface flows when the Euler-Euler approach is considered.

The challenge of the free-surface problem increases when the nature of the liquid and the liquid-gas interface leads to the formation of long thin ligaments, non-detached or migrating satellites or complexity at the pinch-off point. These effects increase when high viscous or viscoelastic fluids come into play.

The main goal of this work was to carry out numerical simulations on disturbed coherent polymeric jets

*Corresponding author. Email: emvalle@usal.es

undergoing controlled Rayleigh instability by applying CFD tools in order to assess the potential of CFD algorithms in solving relatively complex free-surface flows. We compared the results with experiments performed with polymeric solutions, which are less frequently found in the literature of free-surface flow simulations, where mainly Newtonian liquids are investigated.

Previous analyses of the microparticle formation technique (both semiempirical and theoretical approaches) have helped us to predict certain parameters as achieving good system behavior. The selection of an adequate computational method to solve the phenomenon would enable the validation of the theoretical approach and would also predict experimental conditions not easily achievable with our experimental rig. Thus, this study will help us complement our modeling framework by assessing the validity of a particular numerical method and the linked boundary conditions setup.

Reciprocally, the verification of CFD simulations through experiments is fundamental to consolidating these techniques as a reliable tool for studying fluid dynamics. Some recent real cases that compare experimental and simulation results range from large hydraulic structures (Hargreaves, Morvan, & Wright, 2007) to medium-sized channels (Gholami, Akhtari, Minatour, Bonakdari, & Javadi, 2014) to micrometric scales (Fawehinmi, Gaskell, Jimack, Kapur, & Thompson, 2005; Ma et al., 2009).

The simulations in this work were based on a commercial code implementing a Coupled VOF and Level Set (LS) method (CLSVOF) through finite volume technique (ANSYS FLUENT®, release 14.0). The simulated patterns were compared with the experimental results for various operating conditions of instabilization frequencies, amplitudes, viscosities and flow rates.

Similar systems to the one object of this analysis have been studied using VOF, LS, coupling of both and other techniques. Chen, Huang, Kuo, and Chang (2007) studied the parameters affecting the design of an ink droplet generator through a VOF approach, though simulating water rather than ink. They obtained empirical equations based on the simulations for predicting droplet volume and droplet velocity.

Davidson, Harvie, and Cooper-White (2005) used a VOF axisymmetric study for predicting the dynamics of drop formation in flow-focusing microfluidic devices at different flow rates and obtained good qualitative results in terms of the different mechanisms leading to breakup. They studied systems of water-oil (Newtonian liquids). Wang, Liu, Jin, and Cheng (2011) also studied droplet formation in microchannels using the Lattice-Boltzmann Method (LBM).

Furlani and Hanchak (2010) presented a one-dimensional approach to predicting jet nonlinear effects such as instability and satellite formation using the method of lines (MOL) and validated the solutions simulating a water jet and comparing with VOF results.

Pan and Suga (2006) numerically solved Newtonian water-glycerin jets using an LS tracking method capturing the breakup satisfactorily. Castrejón-Pita, Morrison, Harlen, Martin, and Hutchings (2011) used a Lagrangian method to solve the breakup of millimeter-sized water-glycerin Newtonian jets, obtaining good agreement with the experimental results.

Nichita, Zun, and Thome (2010) developed a CLSVOF method to apply in FLUENT® that showed an improved performance concerning the velocity field and surface tension estimation. They studied air/water-sugar, air-oil, and air-water systems.

In general the literature covering the use of VOF and LS as methods of simulating Newtonian fluids is large. Examples of the use of CLSVOF are found in the study of droplet splashing (Yokoi, 2013), drop impact (Ray, Biswas, Sharma, & Welch, 2013), bubble growth and detachment (Albadawi, Donoghue, Delauré, Robinson, & Murray, 2012) and electrospinning of nanofibers (Liu et al., 2014), with an increasing number of published works in the last couple of years. However, simulations describing systems where non-Newtonian fluids take part are less common.

Concerning non-Newtonian studies, Yildirim and Basaran (2001) studied liquid bridges of Newtonian and non-Newtonian fluids considering shear-thinning behavior through the Carreau model. They also collect in their work other computational studies on liquid bridges, which present similarities with liquid jet analysis. Xue, Corvalan, Dravid, and Sojka (2008) also studied Carreau liquid jet evolution with the addition of surfactant transport considerations.

This work addresses the unusual topic of examining non-Newtonian fluid jets by using CFD, how to approach the phenomenon through a CLSVOF model using established commercial software, and some future plans to achieve a more complete analysis for the system.

Experimental equipment and computational domain

The evolution and eventual breakup of capillary jets into still air involve many mechanisms. Surface tension effect, viscoelasticity and aerodynamic interaction are phenomena which are well known to influence the surface instability. Therefore, the formation of microdroplets is influenced by the characteristics of the raw materials and also by the process conditions such as flow rates and instabilization source parameters, which are easy to vary experimentally.

We have performed numerical analysis of laminar jets injected into still air from plain cylindrical nozzles simulating different experimental conditions. Other authors have studied the nature of the destabilization in laminar jets when occurring naturally (Castrejón-Pita, Hoath, & Hutchings, 2012).

In our case, the high viscosity fluid issuing from the nozzle undergoes a destabilizing imposed vibration which

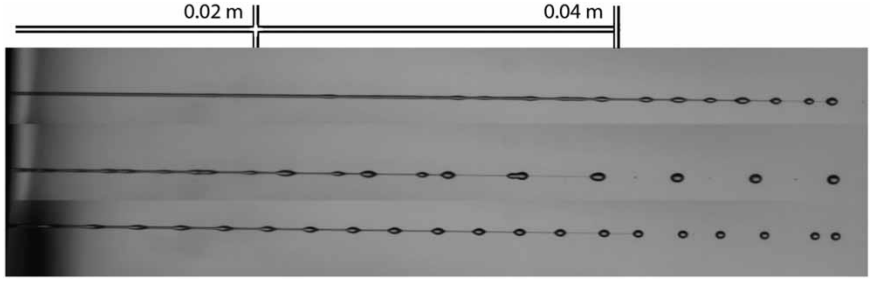

Figure 1. Droplet formation for a 1.3 g/dL sodium alginate solution at a flow rate of 5 mL/min applying from top to bottom a vibration of 0, 800 and 1650 Hz.

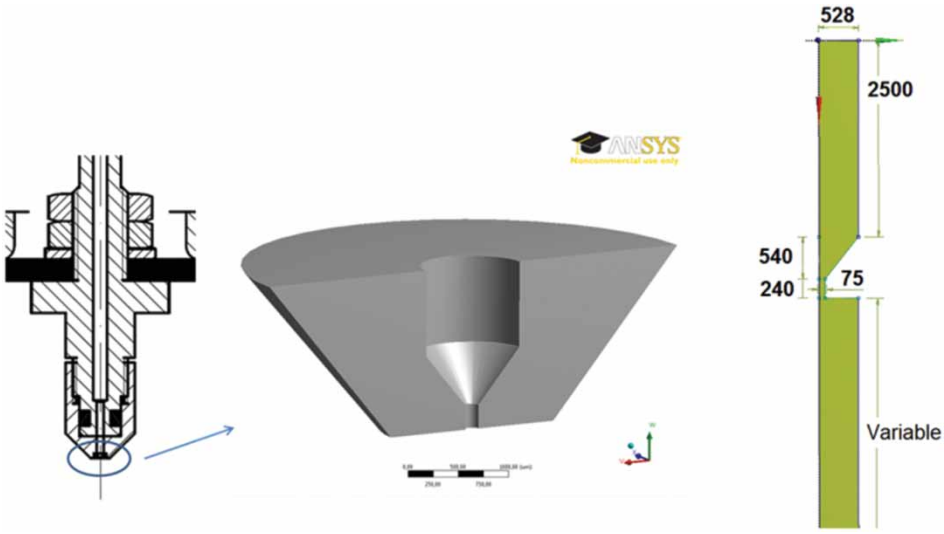

Figure 2. Schematic design of the capillary nozzle (first inset by Nisco Engineering AG®), general axisymmetric design.
Note: Dimensions indicated in μm.

is controlled by the user. The study focuses on a technique that allows the processing of medium-high viscosity fluids by combining a vibrating nozzle with a pressurized system previously characterized by the group (Rodriguez-Rivero et al., 2011).

The evolution of alginate solution jets captured through high-speed camera recordings (Phantom v12.1) shows patterns like those in Figure 1 where sinusoidal axisymmetric waves are observed after the nozzle exit, when controlled disturbances are applied. The visualized structure shows main droplets of solution connected by thin ligaments or threads. The breakup and size are determined by the behavior of these main droplets and the interconnecting ligaments (Bhat et al., 2010; Clasen, Eggers, Fontelos, Li, & McKinley, 2006). Contrary to this type of structure, Newtonian liquid jets show different patterns (Gordon, Yerushalmi, & Shinnar, 1973).

After comparing the 3D and 2D axisymmetric approaches with meshes of similar element size we obtained matching results, suggesting that a 2D axisymmetric approach should be adequate for tackling the problem instead of a more time-consuming 3D calculation. This result was expected given the type of instability, in which the azimuthal velocity component is generally zero.

Thus, the studied cases are considered axisymmetric with respect to the vertical axis, the perturbation being applied vertically through the axis direction and influencing the radial and height components. As mentioned before, external influences in the azimuthal direction are not taken into account since the air is considered still and the capillary nozzle homogenous in shape.

The vibrating system responsible for creating the perturbation corresponds to a commercial module (Nisco Engineering Inc., Zurich, Switzerland) and the selected nozzle mounts a sapphire tip, the inner surface of which has been smoothed to avoid interior roughness.

The geometry consists of a 2D model that comprises part of the microcapillary nozzle, with a 1 mm diameter capillary, a contraction to the final capillary of 150 μm diameter and a surrounded volume downstream sufficient to cover the jet until the breakup (Figure 2). The length and width depend on the case, e.g., for the lowest tested viscosities a geometry of 3 cm in length is enough to cover the evolution of the jet from the growth of the perturbation until the breakup.

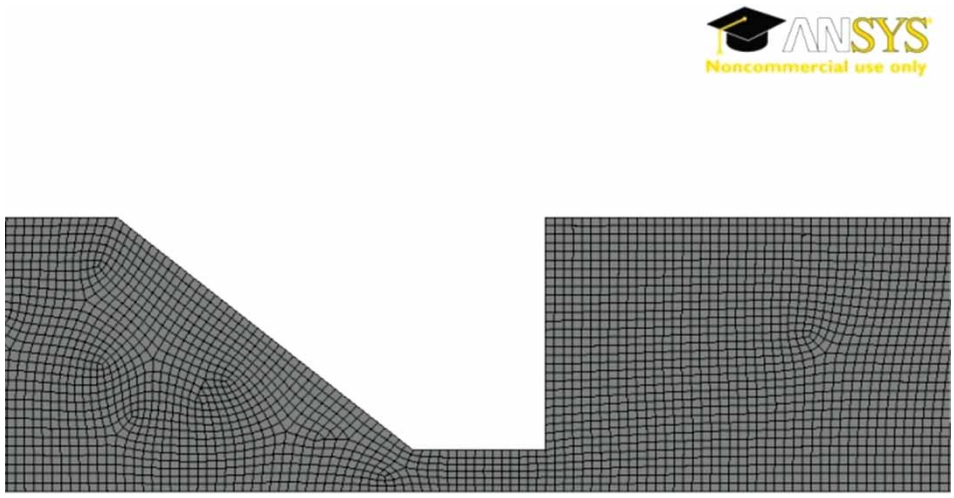

Figure 3. Detail of a quadrilateral-dominant mesh used in the study.

The spatial discretization of the geometry comprises a steady quadrilateral dominant mesh. Mesh independency of the results was assured by decreasing element size and checking the outcomes of repeated simulations. Figure 3 shows a zoomed area of one of the meshes used. The number of cells varies depending on the length of the region considered downwards the nozzle but most of the grids approximately had 298,000 cells (603,000 faces and 305,000 nodes).

In order to solve momentum and continuity equations, a Euler-Euler approach is recommended when the mass of the disperse phase is large, as for the process of laminar jet breakup here tackled (Pfleger and Becker, 2001). Both phases – disperse and continuous – are then treated as interpenetrating continua with separate velocity and temperature fields. Momentum and continuity equations are solved for each phase and a function defines how much of each cell in the grid is occupied by each phase (phasic volume fraction).

Among the Euler-Euler approaches implemented by FLUENT®, the VOF technique is the most commonly used interphase tracking technique when the position of the interphase between two immiscible fluids is of primary importance. FLUENT® now integrates the CLSVOF method.

In VOF the tracking of the interphase between the phases is accomplished by the solution of a continuity equation for the volume fraction of one (or more) of the phases. A single set of momentum equations is shared by the fluids, and the volume fraction of each of the fluids in each computational cell is tracked throughout the domain. The model predicts the location of the interphase and uses single-phase models to predict the flow in each phase.

The continuity equation is then solved for the volume fraction of each phase:

$$\frac{\partial}{\partial t}(\rho_i \alpha_i) + \mathbf{v} \cdot \nabla(\rho_i \alpha_i) = 0, \tag{1}$$

where ρ is the density, α is the volume fraction of fluid i, and v is the fluid velocity.

However, there are difficulties computing accurate local curvatures from the volume fractions, which also involves the computation of the surface-tension force. This requires the use of a fine mesh in order to obtain satisfactory resolution of the interphase (Sussman & Puckett, 2000).

Conversely, the LS method gives better results regarding the computation of the surface tension. In a similar way to VOF, the level set function ϕ gives:

$$\frac{\partial \varphi}{\partial t} + \nabla \cdot (\mathbf{v}\varphi) = 0, \tag{2}$$

and the normal, $\bar{n}$, and curvature, κ, of the interface for computing the surface tension force are defined as:

$$\bar{n} = \frac{\nabla \varphi}{|\nabla \varphi|}, \tag{3}$$

$$\kappa = \nabla \cdot \frac{\nabla \varphi}{|\nabla \varphi|}. \tag{4}$$

However, the LS method is prone to more numerical error and the mass is not conserved. It can be compensated then with the advantage of representing the free surface as volume fractions – provided by VOF – where the mass is conserved.

Some authors have developed and explored the coupling of the LS and VOF methods (Ménard, Tanguy, & Berlemont, 2007; Nichita et al., 2010; Sussman & Puckett, 2000).

A single momentum equation is solved throughout the domain, and the resulting velocity field is shared among the phases. The momentum equation (5) is dependent on the volume fractions of all phases and the computation of surface tension and surface curvature from the level set

function:

$$\frac{\partial}{\partial t}(\rho \mathbf{v}) + \nabla \cdot (\rho \mathbf{v}\mathbf{v}) = -\nabla p + \nabla \cdot \tau - \sigma \kappa \delta(\varphi) + \rho \mathbf{g}, \tag{5}$$

$$\tau = \eta[(\nabla \mathbf{v} + \nabla \mathbf{v}^T)] = \eta \dot{\gamma}, \tag{6}$$

where p is the static pressure, η is the molecular viscosity, τ is the stress tensor, $\dot{\gamma}$ σ is the surface tension coefficient and $\delta(\phi)$ is a function which is also dependent on the grid spacing (ANSYS, 2011). The relationship between shear stress and shear strain described by equation (6) holds for Newtonian fluids. However, for non-Newtonian liquids, equation (6) must be replaced with a more complicated relationship—in this case, equation (8) (see below).

The properties in the equations are determined by the presence of the component phases in each control volume by computing the volume-fraction-averaged properties. For instance the density takes the form of the equation below, where α is the volume fraction of fluid i:

$$\rho = \sum_{i=1}^{n} \rho_i \alpha_i. \tag{7}$$

To investigate further on the theory of coupling and solving using these methods, please refer to the bibliography published by the company that develops the software (ANSYS, 2011).

Model set-up

To determine the flow regime developed in the process, the dimensionless numbers of Ohnesorge, Reynolds and Weber are computed. Most experiments in this work were performed by ejecting alginate solutions from a circular nozzle with a diameter of 150 μm, which results in a cylindrical thread of similar dimensions. The characteristic physical values of the polymer and the process can be considered as a density of 1000 kg/m^3, a surface tension of 0.076 N/m, a viscosity of 1.5 Pa s and a mean velocity of 5 m/s. The surface tension was determined by performing the Du Nouy ring method in a commercial tensiometer (KSV, Sigma 700) and was found to present a very small variation in the range of concentrations tested. The temperature considered for the simulations was 20°C, which was both the mean room temperature during the experiments and the controlled temperature of the solutions.

From the previous values, the following magnitudes are obtained:

$$\mathrm{Oh} = \frac{\eta}{\sqrt{\rho \cdot \sigma \cdot D}} = \frac{1.5}{\sqrt{1000 \cdot 0.076 \cdot 150 \cdot 10^{-6}}} = 14.05,$$

$$\mathrm{Re} = \frac{\rho \cdot v \cdot D}{\eta} = \frac{1000 \cdot 5 \cdot 150 \cdot 10^{-6}}{1.5} = 0.5,$$

$$\mathrm{We} = \frac{\rho \cdot v^2 \cdot D}{\sigma} = \frac{1000 \cdot 5^2 \cdot 150 \cdot 10^{-6}}{0.076} = 49.34,$$

Table 1. Properties of the phases.

Property	Liquid (phase 2 – dispersed)	Gas (phase 1 – continuous)
Material	Sodium alginate	Air
Density (kg/m^3)	998.2	1.225
Viscosity (Pa s)	Carreau–Cross	1.79×10^{-5}
Surface tension (N/m) – (between phases)	0.076	

which corresponds, as expected, to the Rayleigh laminar mechanism. This outcome holds for the whole experimental range examined.

Given the nature of the process and after checking the similitude of the results with 3D cases, axisymmetric simulations in transient mode are considered. Turbulence models and energy or species models are not considered since phenomena such as convection, diffusion, reaction sources and heat transfer do not take place or are of minor importance. Finally, an explicit scheme and pressure-based solver are selected for the simulations (ANSYS, 2011).

The gaseous phase – air – is set as the continuous phase and the polymeric liquid solutions as the dispersed phase. The properties of sodium alginate solution are selected as those of liquid water except for the viscosity model, changing its parameters depending on the case under study. Table 1 briefly presents the main characteristics of both phases.

The most relevant numerical procedures selected are the SIMPLE algorithm for the coupling of pressure and velocity, PRESTO as the pressure interpolation scheme, and least-squares cell-based and second-order accuracy for the computation of gradients and momentum respectively. The Geo-Reconstruct formulation is chosen for the reconstruction of the interface, all of it under a first-order implicit formulation as the time integration scheme. The solver refines the time step automatically, based on the user input for the Courant number. In most of the simulations the mean step size (for a fixed Courant number of magnitude 2) was of the order of 10^{-6} to 10^{-9} s.

For the development of this study we focused on the characterization of the polymeric samples, both under steady-shear measurements in a steady simple-shear flow – covering a range of concentrations up to zero-shear rate viscosities of about 5.5 Pa s – and under dynamic-shear and extensional measurement flow fields in order to determine viscoelasticity parameters (Rodriguez-Rivero, Hilliou, Martín del Valle, & Galán, 2014). With these data we tried to include viscoelastic models through user-defined functions but experienced various difficulties in implementing the code and/or compiling it into FLUENT® and considered then a first study with the use of generalized Newtonian models, relying on the data obtained from the flow curve measurements.

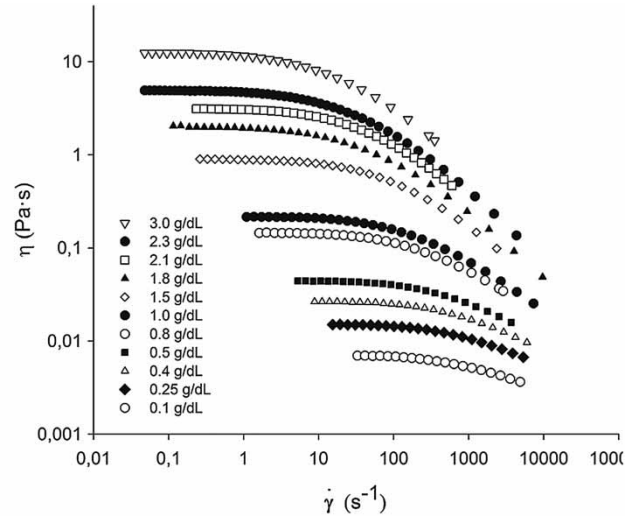

Figure 4. Sodium alginate solutions flow curves – shear viscosity as a function of shear rate.

Figure 4 shows the flow curves obtained from solutions of different concentrations.

Among the most known generalized Newtonian models, the modified constitutive equation of Cross (Barnes, 1989; Cross, 1965) resulted in the best fit for the different flow curves:

$$\frac{\eta - \eta_\infty}{\eta_0 - \eta_\infty} = \frac{1}{1 + (\lambda\dot{\gamma})^{1-n}}, \tag{8}$$

where η_0 is the Newtonian plateau viscosity, λ is the relaxation time, $\dot{\gamma}$ is the strain rate, and the exponent n indicates the power law relation between shear stress and shear rate in the shear-thinning region, which is also known as the flow behavior index. The Newtonian plateaus at large shear rates were considered zero, $\eta_\infty = 0$ (see Table 5).

The conditions of velocity and pressure are introduced through velocity inlet and pressure outlet boundary conditions (BCs). A user-defined function defines a time-dependent velocity accounting for the vibration applied to the nozzle, describing the velocity as sinusoidal with the same frequency as the superimposed vibration (see Nisco Engineering AG®, varD Classic unit for more information). The frequency and amplitude of the vibration is varied and tuned manually with a commercial controller provided as part of the commercial device. This is described in the equation below, where V is the velocity of the fluid without considering the perturbation, A is the velocity amplitude, ω is the angular frequency and f is the applied frequency:

$$v_x(t) = V + A\sin(2\pi\,\mathrm{ft}). \tag{9}$$

Table 3. Different amplitude conditions for the simulations for an approximate flow rate of 5.5 mL/min.

Velocity inlet expression	
$v_x(t) = 0.1 + 0.001\sin(2\pi \cdot 1000 \cdot t)$	*(3.a)*
$v_x(t) = 0.1 + 0.010\sin(2\pi \cdot 1000 \cdot t)$	*(3.b)*
$v_x(t) = 0.1 + 0.050\sin(2\pi \cdot 1000 \cdot t)$	*(3.c)*
$v_x(t) = 0.1 + 0.075\sin(2\pi \cdot 1000 \cdot t)$	*(3.d)*
$v_x(t) = 0.1 + 0.100\sin(2\pi \cdot 1000 \cdot t)$	*(3.e)*

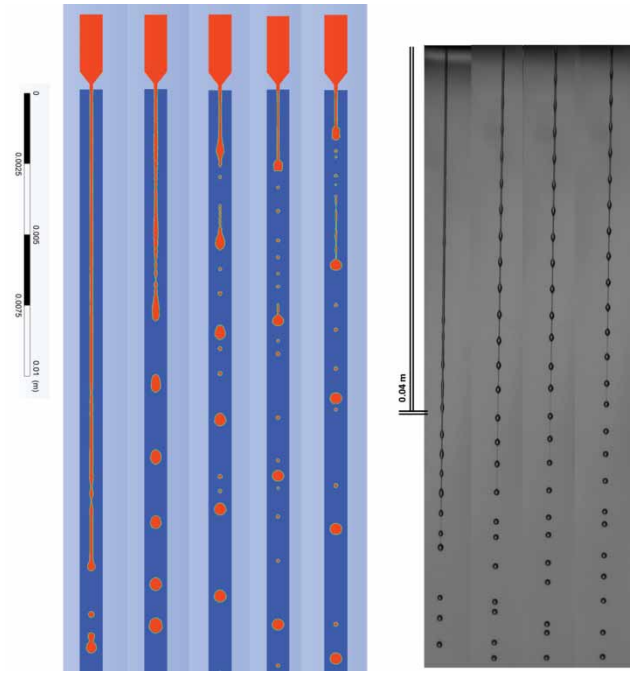

Figure 5. Phase profiles for a 1.3 g/dL sodium alginate solution at 5.5 mL/min.
Note: Left: from numerical simulations (amplitudes of the disturbing wave from 0.001 to 0.1 m/s). Right: from experiments applying a vibration of 1 kHz with different amplitude conditions of 0, 40, 80, and 100%.

Table 4. Different frequency conditions for the simulations.

Velocity inlet expression	
$v_x(t) = 0.1 + 0.01\sin(2\pi \cdot 1000 \cdot t)$	*(4.a)*
$v_x(t) = 0.1 + 0.01\sin(2\pi \cdot 2000 \cdot t)$	*(4.b)*
$v_x(t) = 0.1 + 0.01\sin(2\pi \cdot 3000 \cdot t)$	*(4.c)*

Table 2. Jet velocity and velocity to apply at the inlet BC for the tested flow rates.

Flow rate (mL/min)	5	5.5	6	6.5	7	7.5	8
Inlet BC velocity (m/s)	0.095	0.105	0.114	0.124	0.133	0.143	0.152
		Figures 5–8		Figure 8		Figure 8	Figure 8

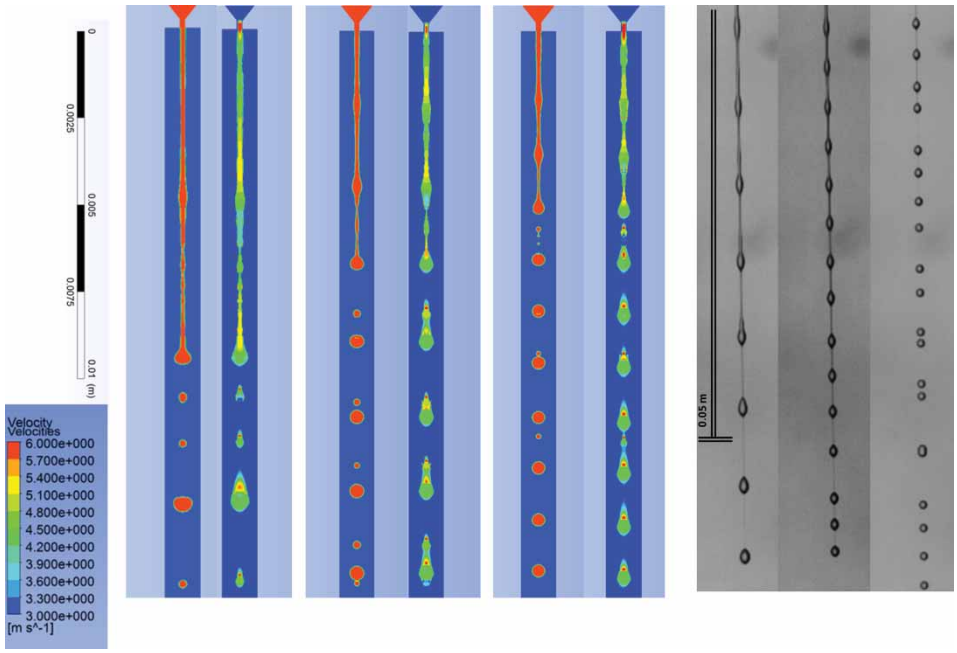

Figure 6. Phase and velocity profiles for different frequencies of the disturbing wave. Note: 1.6 g/dL at approximately 5.5 mL/min.

Table 5. Rheological characteristics of the solutions of different concentrations.

Concentration (g/dL)	0.4	1.3	1.6	1.8	2.0
Zero-shear viscosity (Pa s)	0.310	0.709	1.320	2.032	2.744
n	0.227	0.230	0.250	0.278	0.242
λ (s)	3.2×10^{-3}	4.6×10^{-3}	8.5×10^{-3}	0.0169	0.0175
	Figure 7 *(5.a)*	Figures 5 and 7 *(5.b)*	Figures 6–8 *(5.c)*	Figure 7 *(5.d)*	Figure 7 *(5.e)*

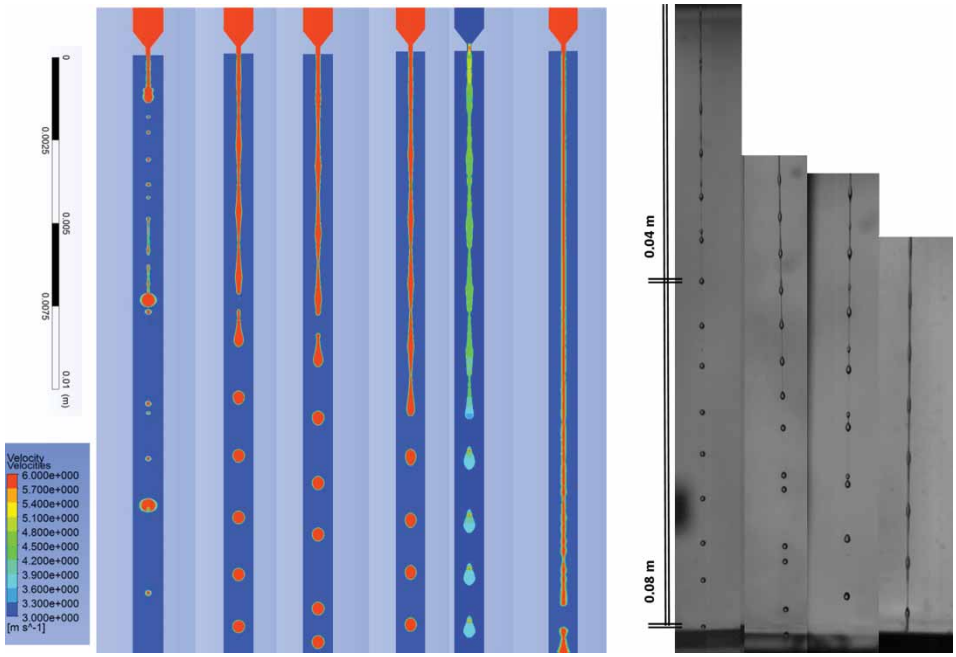

Figure 7. (left) Phase profiles and experimental snapshots for different solution concentrations (Table 5).
Note: Left: Phase profiles at 5.5 mL/min. Right: Experimental snapshots for concentrations 1.3 (0.709 Pa s), 1.6 (1.320 Pa s), 1.8 (2.032 Pa s), and 2.0 (2.744 Pa s) g/dL.

Table 6. Jet velocity and velocity to apply at the inlet BC for the tested flow rates.

Flow rate (mL/min)	5	5.5	6	6.5	7	7.5	8
Jet diameter (μm)	200.0	188.2	175.7	173.2	171.4	170.8	164.2
Jet mean velocity (m/s)	2.65	3.30	4.12	4.60	5.06	5.45	5.90
Inlet BC velocity (m/s)	0.095	0.105	0.114	0.124	0.133	0.143	0.152

Table 7. Flow rate conditions for the simulations.

Inlet BC flow rate (mL/min)	Velocity inlet expression		Resulting flow rate (mL/min)
3.5	$v_x(t) = 0.060 + 0.01 \sin(2\pi \cdot 1500 \cdot t)$	*(7.a)*	5
4	$v_x(t) = 0.080 + 0.01 \sin(2\pi \cdot 1500 \cdot t)$	*(7.b)*	5.5
6.5	$v_x(t) = 0.124 + 0.01 \sin(2\pi \cdot 1500 \cdot t)$	*(7.c)*	7.5
7.5	$v_x(t) = 0.143 + 0.01 \sin(2\pi \cdot 1500 \cdot t)$	*(7.d)*	9
8	$v_x(t) = 0.152 + 0.01 \sin(2\pi \cdot 1500 \cdot t)$	*(7.e)*	> 9

The mean velocity V in equation (9) is computed from a known flow rate and the area of the inlet boundary as $Q_{jet} = A_{inlet}V$. Table 2 collects the computed velocities for the 1 mm capillary before the nozzle (inlet).

Results and discussion

The effects of the viscosity, flow rate and disturbing frequency – parameters that have been verified as influencing the evolution of the jet instability – are examined. The effect of the amplitude of the disturbing wave is also considered.

A qualitative assessment of the simulations is pursued through comparison with experimental images in order to verify the behavior of the model. In general, as a first approach, initial qualitative analyses based on relatively simple models, in terms of viscosity for instance, are typically conducted (see the Introduction above). Thus, we intend to assess the behavior of the CLSVOF model when dealing with the newly developed experimental process and the use of medium-high viscosity polymers with a relatively simple constitutive equation, not considering the elastic effects of the polymer. A more quantitative approach will be studied in further works by including the viscoelastic nature of the polymer through more complex constitutive equations.

Effect of amplitude and frequency

As explained above, the value of the frequency f in equation (9) is selected as the output frequency applied from the experimental controller. However, a specific value for the amplitude is unknown. To determine the most suitable value for the amplitude different simulations were carried out for a solution of 1.3 g/dL (see Table 5 for rheological data).

Table 3 lists the applied inlet BC expressions assuming an approximate flow rate of 5.5 mL/min. The resulting images showing phase volume fractions are collected in

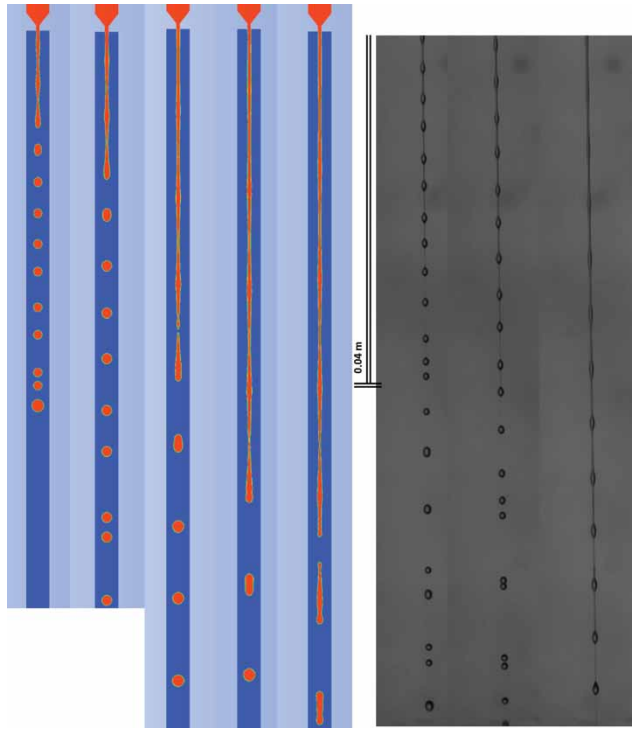

Figure 8. Phase profiles for different flow rates for a concentration of 1.6 g/dL, experimental snapshots of 1.6 g/dL at 5.5, 6, and 7.5 mL/min.

Figure 5, which shows results from the numerical simulations and snapshots from experimentation. It can be observed that when the amplitude of the disturbing wave increases, the jet breaks in a shorter length, as seen in the experiments. However, it is also clear that the breakup lengths of the alginate jets in the experimental snapshots are longer than those in the simulations with Generalized Newtonian models (GNMs).

After analyzing the results, an amplitude of 0.01 m/s was chosen for carrying out the simulations that followed. This value was chosen for presenting intermediate breakup lengths, as well as its clear sinusoidal growth profile and the lack of excessive satellite droplets. Moreover, the

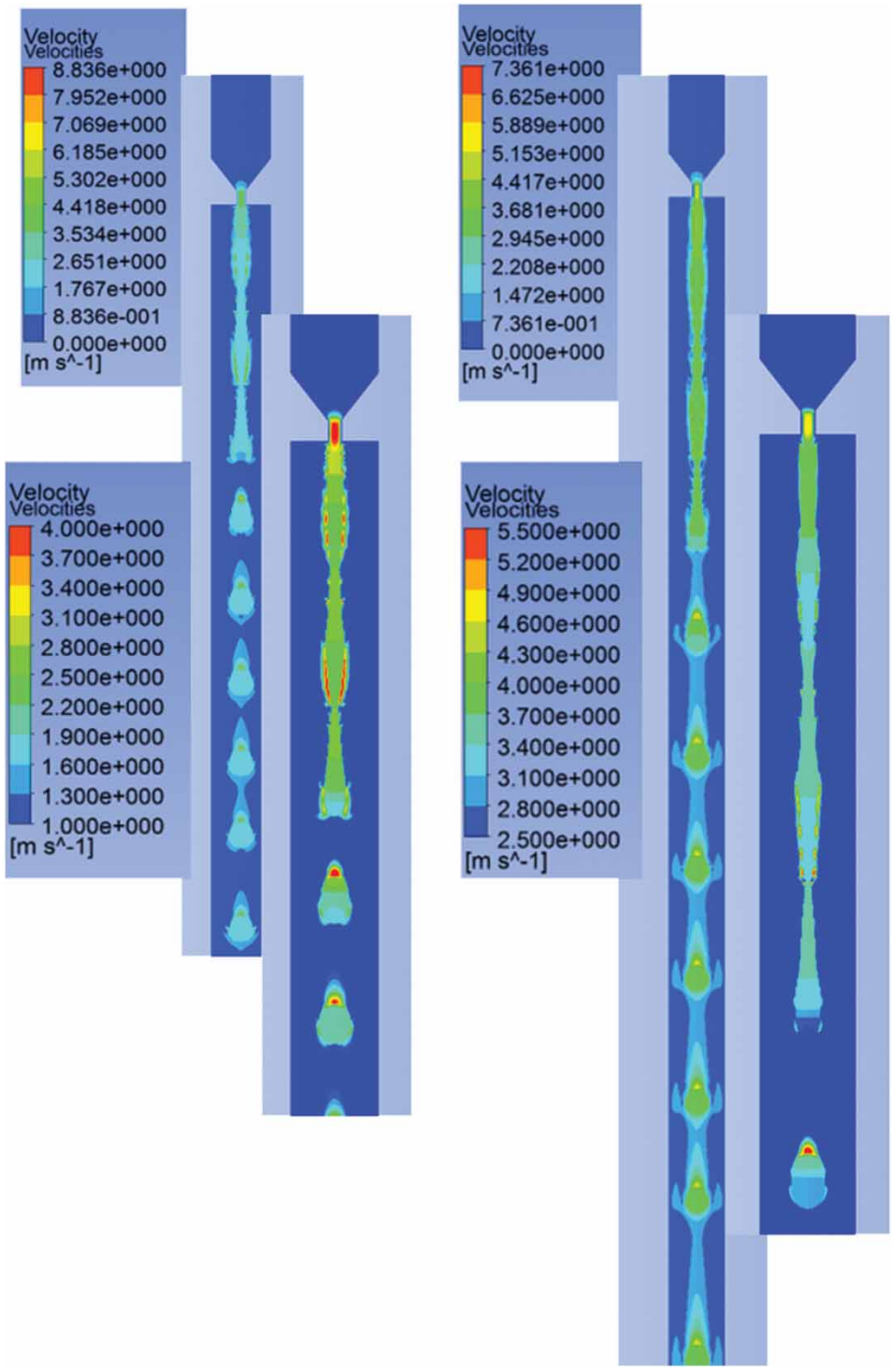

Figure 9. Velocity profiles comparing different flow rates (Table 7).

simulations with higher amplitudes highly overestimate the jet velocity compared with the experimentally measured values.

Once the amplitude was set, the effect of applying different frequencies was investigated. Table 4 lists the different applied conditions. Figure 6 compares experimental and simulated images for a solution of concentration 1.6 g/dL (see Table 5 for rheological data).

The results from the simulations and experiments in Figure 6 match in showing shorter breakup lengths and closer and smaller droplets when the frequency of the disturbing wave increases.

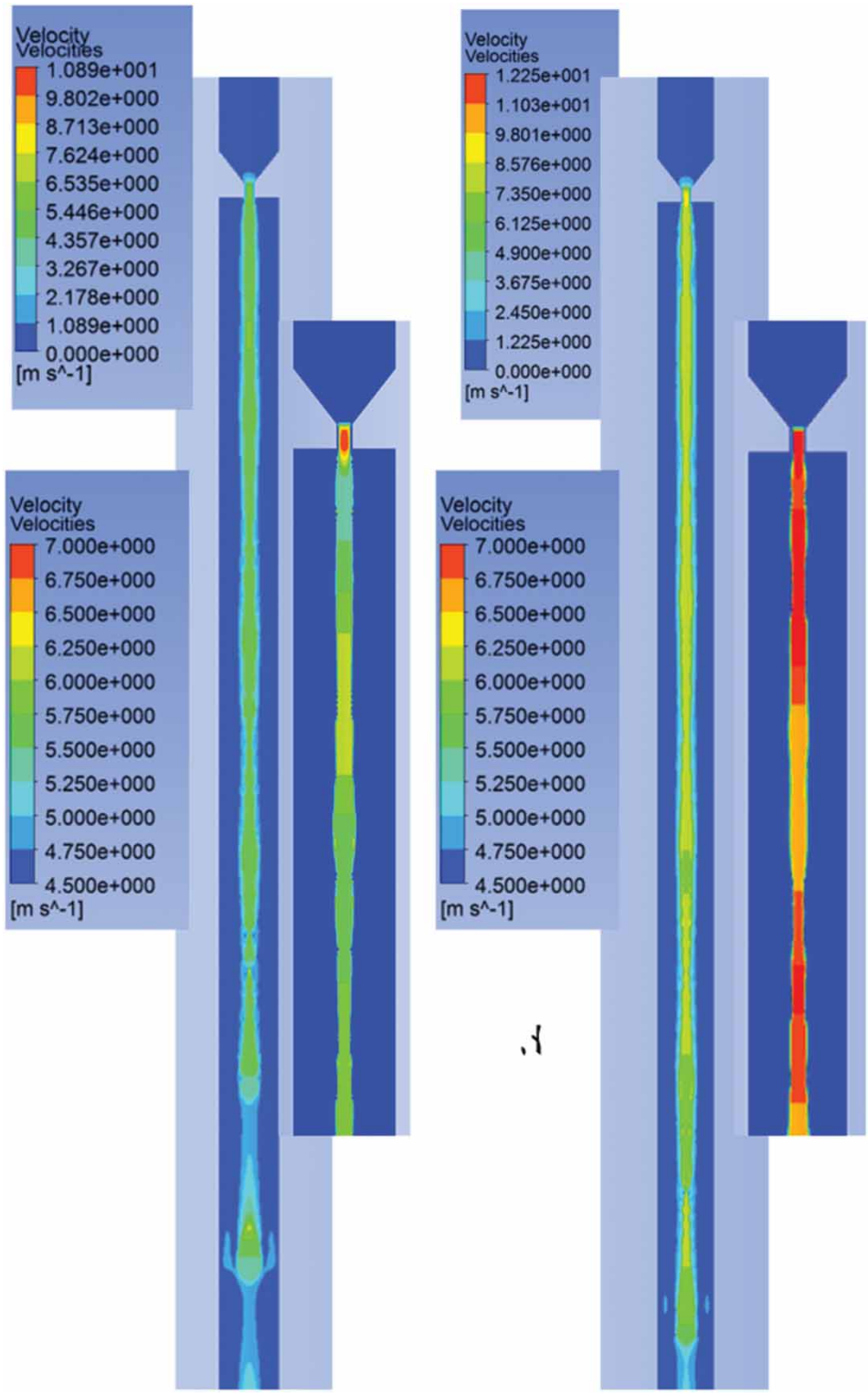

Figure 10. Velocity profiles comparing different flow rates (Table 7).

It is worth mentioning that the droplet spacing is not consistent between the experiments and the simulations, not showing uniform spacing in the former case. There might be different reasons why the droplet spacing captured experimentally is not uniform. The nonlinear evolution of viscoelastic jets involves the acceleration and deceleration of droplets, due mainly to tensile stresses and different behavior along the interconnecting ligaments, leading to

non-uniform spacing between the main droplets. Moreover, the shear and extensional stresses, as well as the elasto-capillary balance along the jet, vary due to the different shape that the jet experiences, changing the viscosity (particularly the extensional viscosity), and thus the fluid dynamics behavior along the jet.

Since viscoelastic effects are not accounted for in the simulations, the elastic stresses do not influence the evolution. In addition, the non-presence of ligaments and a breakup in a shorter time and length in the simulations mean that the main droplets do not suffer such different effects in their acceleration.

Furthermore, the formation of the small droplets which seems to replace the ligaments observed in the experiments might be due to the obtaining of parasitic currents that generate spurious drops by the model, as previously reported by Lafaurie, Nardone, Scardovelli, Zaleski, and Zanetti (1994). Further work should be addressed in this direction in order to assess whether this is due to the numerical scheme, or if it could be at least partially solved with a different meshing approach for instance.

Effect of viscosity

The effect of changing the concentration of the samples was analyzed by applying the inlet condition $v_x(t) = 0.1 + 0.01 \sin(2\pi \cdot 1000 \cdot t)$. The analysis involved the different viscosity conditions collected in Table 5.

Figure 7 shows how an increase in the concentration stabilizes the jet by delaying its breakup, as predicted by the experiments and by instability theories (Bogy, 1979).

Effect of the flow rate

The effect of the flow rate is assessed through the change in the mean velocity V (equation (9)). Table 6 lists the magnitudes of the mean measured velocities for the range of concentrations considered and the applied mean velocities at the inlet BC.

Table 7 presents the conditions introduced in the simulations for a 1.6 g/dL solution (first column) and Figures 8–10 present the phase and velocity profiles obtained under those conditions. From Figure 8 it can be observed that the higher the flow rate, the longer the breakup length for both simulated and experimental results.

The obtained simulated velocities (see Figures 9 and 10) are overestimated compared to the expected values from the computation, thereby matching with higher values of flow rates, as displayed in the second column of Table 7.

Conclusions

This study confirms the capability of the selected CLSVOF model to successfully track the interface of a capillary unstable jet and capture its breakup. The simulations showed good qualitative results, in agreement with the tendencies observed in the experimental work.

This computational study was compared to an experimental technique using non-Newtonian viscoelastic samples. However, the numerical solutions used generalized Newtonian models, accounting for the shear-thinning nature of the polymer but not accounting for the characteristic effects of the viscoelasticity on the instability and the droplet formation from polymeric jets, as seen in the experimental images. This limitation highlights the need for considering the effects of the polymer elasticity as key in the Rayleigh instability. Therefore, and as a future direction for this work, the inclusion of viscoelastic models in the simulations must be addressed in order to obtain the relevant qualitative results to predict system behavior, such as droplet size and breakup length.

However, it can be concluded that the use of the CLSVOF model with relatively simple meshes and the presented set-up deals reasonably well with interface tracking, which makes it adequate for the study of capillary laminar instabilities.

Disclosure statement

No potential conflict of interest was reported by the author(s).

Funding

This work was supported by the European Research Council (ERC) Project MYCAP (258984) Starting Grants 2010. Cristina Rodriguez-Rivero was supported by a ‘Formacion del Profesorado Universitario’ (FPU) fellowship from the Ministry of Education of Spain.

References

Albadawi, A., Donoghue, D. B., Delauré, Y. M. C., Robinson, A. J., & Murray, D. B. (2012). Numerical investigation of volume of fluid and level set interface capturing methods for bubble growth and detachment. *Journal of Physics: Conference Series*, *395*(1), 012166 (8).

Alderliesten, M. (2004). Mean particle diameters. Part IV: Empirical selection of the proper type of mean particle diameter describing a product or material property. *Particle & Particle Systems Characterization*, *21*(3), 179–196.

ANSYS, I. (2011). ANSYS FLUENT theory guide. Release 14.0. ANSYS, Inc.

Barnes, H. A. (1989). Shear-thickening (“Dilatancy”) in suspensions of nonaggregating solid particles dispersed in Newtonian liquids. *Journal of Rheology*, *33*(2), 329–366.

Benita, S. (Ed.). (2006). *Microencapsulation: Methods and industrial applications* (2nd ed.). Florida, FL: Taylor & Francis Group.

Bhat, P. P., Appathurai, S., Harris, M. T., Pasquali, M., McKinley, G. H., & Basaran, O. A. (2010). Formation of beads-on-a-string structures during break-up of viscoelastic filaments. *Nature Physics*, *6*, 625–631.

Bogy, D. B. (1979). Drop formation in a circular liquid jet. *Annual Review of Fluid Mechanics*, *11*(1), 207–228.

Castrejón-Pita, J. R., Hoath, S. D., & Hutchings, I. M. (2012). Velocity profiles in a cylindrical liquid jet by reconstructed velocimetry. *J. Fluids Eng.*, *134*(1), 011201 (13).

Castrejón-Pita, J. R., Morrison, N. F., Harlen, O. G., Martin, G. D., & Hutchings, I. M. (2011). Experiments and Lagrangian simulations on the formation of droplets in continuous mode. *Phys. Rev. E*, *83*, 016301 (10).

Cerveró, J. M., Nogareda, J., Valle, E. M. M., & Galán, M. A. (2011). Development of a technology to produce monodispersed microparticles based on the formation of drops from viscous non-Newtonian liquids sprayed through a fan jet nozzle. *Chemical Engineering Journal*, *174*(2–3), 699–708.

Clasen, C., Eggers, J., Fontelos, M. A., Li, J., & McKinley, G. H. (2006). The beads-on-string structure of viscoelastic threads. *Journal of Fluid Mechanics*, *556*, 283–308.

Chan, L. W., Tan, L. H. and Heng, P. S. (2008). Process analytical technology: Application to particle sizing in spray drying. *AAPS PharmSciTech*, *9*(1), 259–266.

Chen, Y. S., Huang, Y. L., Kuo, C. H., & Chang, S. H. (2007). Investigation of design parameters for droplet generators driven by piezoelectric actuators. *International Journal of Mechanical Sciences*, *49*(6), 733–740.

Chigier, N. A., & Reitz, R. D. (1996). Regimes of Jet Breakup and Breakup Mechanisms (Physical Aspects) Recent Advances in Spray Combustion: Spray Atomization and Drop Burning Phenomena. January, 109–135.

Cross, M. M. (1965). Rheology of non-Newtonian fluids: A new flow equation for pseudoplastic systems. *Journal of Colloid Science*, *20*(5), 417–437.

Davidson, M. R., Harvie, D. J. E., & Cooper-White, J. J. (2005). Flow focusing in microchannels. *ANZIAM Journal*, *46*(E), C47–C58.

Eggers, J. (2014). Instability of a polymeric thread. *Physics of Fluids*, *26*(3), 033106 (9).

Eggers, J., & Villermaux, E. (2008). Physics of liquid jets. *Reports on Progress in Physics*, *71*, 036601 (79).

Fawehinmi, O., Gaskell, P., Jimack, P., Kapur, N., & Thompson, H. (2005). A combined experimental and computational fluid dynamics analysis of the dynamics of drop formation. *Proceedings of the Institution of Mechanical Engineers, Part C: Journal of Mechanical Engineering Science*, *219*(9), 933–947.

Furlani, E. P., & Hanchak, M. S. (2010). Nonlinear analysis of the deformation and breakup of viscous microjets using the method of lines. *International Journal for Numerical Methods in Fluids*, *65*(5), 563–577.

de Gans, B. J., Duineveld, P. C., & Schubert, U. S. (2004). Inkjet printing of polymers: State of the art and future developments. *Advanced Materials*, *16*(3), 203–213.

Gholami, A., Akhtari, A. A., Minatour, Y., Bonakdari, H., & Javadi, A. A. (2014). Experimental and numerical study on velocity fields and water surface profile in a strongly-curved 90° open channel bend. *Engineering Applications of Computational Fluid Mechanics*, *8*(3), 447–461.

Goedde, E. F., & Yuen, M. C. (1970). Experiments on liquid jet instability. *Journal of Fluid Mechanics*, *40*(03), 495–511.

Gordon, M., Yerushalmi, J., & Shinnar, R. (1973). Instability of jets of non-Newtonian fluids. *Transactions of the Society of Rheology*, *17*(2), 303–324.

Hargreaves, D. M., Morvan, H. P., & Wright, N. G. (2007). Validation of the volume of fluid method for free surface calculation: The broad-crested weir. *Engineering Applications of Computational Fluid Mechanics*, *1*(2), 136–146.

Hirt, C. W., & Nichols, B. D. (1981). Volume of fluid (VOF) method for the dynamics of free boundaries. *Journal of Computational Physics*, *39*(1), 201–225.

Javadi, A., Eggers, J., Bonn, D., Habibi, M., & Ribe, N. M. (2013). Delayed capillary breakup of falling viscous jets. *Physical Review Letters*, *110*(14), (4).

Lafaurie, B., Nardone, C., Scardovelli, R., Zaleski, S., & Zanetti, G. (1994). Modelling merging and fragmentation in multiphase flow with SURFER. *Journal of Computational Physics*, *113*, 134–147.

Liu, Y., Li, J., Tian, Y., Yu, X., Liu, J., & Zhou, B. (2014). CLSVOF method to study the formation process of Taylor cone in crater-like electrospinning of nanofibers. *Journal of Nanomaterials*, *14*, 12 pages.

Ma, B., Ruwet, V., Corieri, P., Theunissen, R., Riethmuller, M., & Darquenne, C. (2009). CFD simulation and experimental validation of fluid flow and particle transport in a model of alveolated airways. *Journal of Aerosol Science*, *40*(5), 403–441.

Ménard, T., Tanguy, S., & Berlemont, A. (2007). Coupling level set/VOF/ghost fluid methods: Validation and application to 3D simulation of the primary break-up of a liquid jet. *International Journal of Multiphase Flow*, *33*(5), 510–524.

Nichita, B. A., Zun, I., & Thome, J. R. (2010). A level set method coupled with a volume of fluid method for modeling of gas-liquid interface in Bubbly flow. *Journal of Fluids Engineering*, *132*(8), 081302–081302.

Pan, Y., & Suga, K. (2006). A numerical study on the breakup process of laminar liquid jets into a gas. *Physics of Fluids*, *18*(5), 052101 (11).

Pfleger, D., & Becker, S. (2001). Modelling and simulation of the dynamic behaviour in a bubble column. *Chemical Engineering Science*, *56*, 1737–1747.

Plateau, J. (Ed.). (1873). *Statique expérimentale et théorique des liquides soumis aux seules forces moléculaires*. Paris: Gauthier-Villars.

Ray, B., Biswas, G., Sharma, A., & Welch, S. W. J. (2013). CLSVOF method to study consecutive drop impact on liquid pool. *International Journal of Numerical Methods for Heat & Fluid Flow*, *23*(1), 143–158.

Reitz, R. D., & Bracco, F. V. (1986). Mechanisms of breakup of round liquids jets. In N. Cheremisnoff (Ed.), *The encyclopedia of fluid mechanics* (Vol. 3, Chapter 10, pp. 233–249). Texas: Houston.

Rodríguez-Rivero, C., Del Valle, E. M. M., & Galán, M. A. (2011). Development of a new technique to generate microcapsules from the breakup of non-Newtonian highly viscous fluid jets. *AIChE Journal*, *57*(12), 3436–3447.

Rodríguez-Rivero, C., Hilliou, L., Martín del Valle, E. M., & Galán, M. A. (2014). Rheological characterization of commercial highly viscous alginate solutions in shear and extensional flows. *Rheologica Acta*, *53*(7), 559–570.

Savart, F. (1833). Mémoire sur la constitution des veines liquides lancées par des orifices circulaires en mince paroi. *Annali di Chimica*, *53*, 337–386.

Song, H., Chen, D. L., & Ismagilov, R. F. (2006). Reactions in droplets in microfluidic channels. *Angewandte Chemie International Edition*, *45*(44), 7336–7356.

Srinivasan, V., Pamula, V. K., & Fair, R. B. (2004). An integrated digital microfluidic lab-on-a-chip for clinical diagnostics on human physiological fluids. *Lab on a Chip*, *4*(4), 310–315.

Sterling, A. M., & Sleicher, C. A. (1975). The instability of capillary jets. *Journal of Fluid Mechanics*, *68*(03), 477–495.

Sussman, M., & Puckett, E. G. (2000). A coupled level set and volume-of-fluid method for computing 3D and axisymmetric incompressible two-phase flows. *Journal of Computational Physics*, *162*(2), 301–337.

Wang, W., Liu, Z., Jin, Y., & Cheng, Y. (2011). LBM simulation of droplet formation in micro-channels. *Chemical Engineering Journal*, *173*(3), 828–836.

Weber, C. (1931). Zum Zerfall eines Flüssigkeitsstrahls. *Zeit für angewandte Mathematik und Mechanik*, *11*, 136–154.

Xue, Z., Corvalan, C. M., Dravid, V., & Sojka, P. E. (2008). Breakup of shear-thinning liquid jets with surfactants. *Chemical Engineering Science*, *63*(7), 1842–1849.

Yildirim, O. E., & Basaran, O. A. (2001). Deformation and breakup of stretching bridges of Newtonian and shear-thinning liquids: comparison of one- and two-dimensional models. *Chemical Engineering Science*, *56*(1), 211–233.

Yokoi, K. (2013). A practical numerical framework for free surface flows based on CLSVOF method, multi-moment methods and density-scaled CSF model: Numerical simulations of droplet splashing. *Journal of Computational Physics*, *232*(1), 252–271.

Zimmermann, U., Cramer, H., Jork, A., Thürmer, F., Zimmermann, H., Fuhr, G., Hasse, C., & Rothmund, M. (2001). Microencapsulation-based cell therapy. *Biotechnology Set*, Second Edition (eds H.-J. Rehm and G. Reed), Wiley-VCH Verlag GmbH, Weinheim, Germany. (pp. 547–571).